Realisation of an optical pressure standard by a multi-reflection interferometric technique

(Article begins on next page)

25 April 2024

Realisation of an optical pressure standard by a multi-reflection interferometric technique

D. Mari [*], M. Pisani, M. Astrua, M. Zucco, S. Pasqualin, A. Egidi, M. Bertinetti, A. Barbone

Istituto Nazionale di Ricerca Metrologica (INRIM), Strada delle Cacce 91, 10135 Torino, Italy

A B S T R A C T

A novel realization of an optical pressure standard, alternative to Fabry-Perot cavity-based techniques, is presented. It is based on the measurement of the refractive index of a gas through an unbalanced homodyne interferometer, designed to have one of its two arms formed by a multi reflection double mirror assembly to establish an unbalance length larger than 6 m in a compact setup.

The paper illustrates the most important steps concerning its realization: the estimate of the pressure-induced deformation of the interferometer, the temperature control at millikelvin level and the measurement in vacuum of the unbalance of the interferometer.

The evaluation of the uncertainty of the realized optical pressure standard currently demonstrated to fulfill the main goal of having the ability to measure pressure with a relative uncertainty of 10 ppm at 100 kPa.

1. Introduction

Current conventional realisations of the pascal in gas medium rely on different techniques, depending on the pressure range, including pressure balances [1–3] and mercury manometers [4–5]. For pressure below 1 kPa, further methods involving static or continuous expansion of gases [6–9] are commonly used, though considerably increase the effort needed for measurement operation. In addition, the performance of traditional realizations has remained basically the same over the last decade and they suffer from practical and environmental limitations. For instance, the mercury manometers are the only conventional standards which are able to cover the whole pressure range between 100 Pa and 120 kPa, but they are progressively abandoned, due to presence of mercury, not in line with Word Health Organization resolutions recommending the progressive reduction of human exposure to mercury and mercury compounds [10].

Accordingly, the piston gauges are frequently replacing mercury manometers, establishing a common realization of the pascal based on "force per area", directly related to usual definition of pressure.

The 26th General Conference on Weights and Measures (16th November 2018) adopted a revision of the International System of Units (SI). The new SI, in effect since May 2019, is based on established values of several fundamental physical constants and encourages the exploration of new paths for vacuum and pressure measurements, starting from the fundamental laws and constants of physics. In the new SI, the uncertainty of the Boltzmann constant k_B was eliminated, making advantageous to realise the pascal through number density measurements via optical methods, instead of "force per area" measurements, with the aim of establishing a quantum-based traceability route to the pascal.

The realization of "optical" pascal is currently an emerging research topic where significant progress has been made in recent years at several metrological institutes and universities all around the world [11–26].

In such a contest, the performance of this novel generation of photon-based pressure standards, in long term, would be mainly limited by the accuracies of quantum calculations of gas parameters and the gas temperature determination.

The paper reports the current progress at INRIM in the optical realization of the pascal through the measurement of the refractive index of a gas by the a multi-reflection interferometer, named UINT, which was developed in the framework of the EMPIR project 18SIB04 "QuantumPascal".

The UINT-based technique, as the Fabry-Perot cavity-based technique, relies on the measurement of gas number density by using the Lorentz-Lorenz equation, in accordance with the new definition of SI.

2. Theory

The realization of the pascal through the number density ρ_N requires

---

a formula relating ρ_N to the standard pressure p. For an ideal gas, p can be determined applying the ideal gas law:

$$p = \rho_N k_B T \tag{1}$$

in which is the number density ρ_N is the number of molecules N per volume V, k_B is the Boltzmann constant and T is the temperature. However, the approximation for ideal gas is not sufficient to realize an accurate pressure standard by optical methods, i.e. it is necessary to consider an equation describing the real gas behaviour, in which the molecules interact through Van der Waals forces, their mutual collisions are not purely elastic and evidenced a not negligible proper volume. Introducing the molar density ρ and the molar gas constant R, for a real gas, p can be written through a virial expansion in the molar density:

$$p = \rho R T (1 + B\rho + C\rho^2 + \cdots) \tag{2}$$

where R is the product of Boltzmann constant k_B and the Avogadro number N_A, B and C are respectively the second and third order density virial coefficients. It should be noted that the equation (2) "contains" the constants k_B and N_A, defined in the new SI as constant with exact values and no uncertainties.

To have an example of the importance of considering real gas effects, in case of nitrogen at 100 kPa, neglecting the second term of equation (2) would mean making a relative error on the pressure value equal to about 160 ppm, which is not acceptable for an accurate pressure standard with a target relative standard uncertainty of 10 ppm at 100 kPa.

Once determined the relationship between p and ρ, the latter can be determined through the Lorentz-Lorenz equation, by the measurement of the gas refractive index n:

$$\frac{n^2 - 1}{n^2 + 2} = \rho(A_R + B_R\rho + C_R\rho^2 + \cdots) \tag{3}$$

where A_R is the molar polarizability, B_R and C_R are the second and third order refractivity virial coefficients, which, similarly to density virial coefficients in equation (2), take into account the non-linearity effects.

The refractive index n is thus measured by means of the UINT interferometer which basically operates as a refractometer:

$$n = n_{vac} + \frac{\varphi\lambda}{L} \approx 1 + \frac{\varphi\lambda}{L} \tag{4}$$

where n_{vac} is the refractive index in vacuum condition, i.e. the reference condition of the system at residual pressure p_{res}, typically not exceeding $5 \cdot 10^{-2}$ Pa, φ is the number of interference fringes occurred between the initial pressure p_{res} and p, λ is the laser wavelength and L is the total unbalance of the interferometer under vacuum, i.e. the optical path difference between reference and measurement arm of the interferometer, considering the forward and backward optical path. It should be noted that the approximation $n_{vac} \approx 1$, at the limit value of residual pressure $5 \cdot 10^{-2}$ Pa, can be accepted only for standard pressure above 50 kPa, where the effect of the approximation is in the sub-ppm range.

The standard pressure can be rewritten in terms of a power series of the refractivity (n-1), eliminating the quantity ρ, making use of equations (2) and (3) [11] and maintaining the terms until the third order:

$$p = z_1(n-1) + z_2(n-1)^2 + z_3(n-1)^3 \tag{5}$$

in which the coefficient z_1, z_2 and z_3 are given by:

$$z_1 = \frac{2RT}{3A_R}$$

$$z_2 = \frac{RT}{9A_R^3}(-A_R^2 + 4A_R B - 4B_R) \tag{6}$$

$$z_3 = \frac{4RT}{27A_R^5}(-A_R^4 - A_R^3 B + A_R^2 B_R + 4A_R BB_R + 4AB_R^2 + 2A_R^2 C - 2A_R C_R)$$

The equation (5), limited to the third order terms, completely satisfies the aims of the work presented in this article, as allows to assess the pressure with a relative error, with respect to the Lorentz-Lorenz equation (3), which is less than 1 ppm.

3. Method and system

The quantum-based method developed to realize the optical pressure standard relies on the measurement of the refractive index of a gas by means of a strongly unbalanced Michelson interferometer used as a refractometer [19,21,22,27].

The Fig. 1 shows the schematic of the system, a homodyne Michelson laser interferometer with fixed arms. The light source is a frequency stabilized He-Ne laser (wavelength $\lambda \approx 633$ nm), coupled to a polarization maintaining fiber ending with a collimator FC to launch the radiation in the interferometer. The heart of the optical system is the double mirror multiplication set-up in the measurement arm, where the beam is reflected several times between two quasi-parallel mirrors A and B.

The double mirror assembly acts basically like as a single plane mirror reflecting back the laser beam allowing to obtain a number N of reflections depending both on the incidence angle on mirror A and the angle between mirrors A and B [27].

The reference beam coming from the reference mirror MR and the measurement beam are recombined by the beam splitter BS1 where interference takes place. After passing through a polarizer P and a further beam splitter BS2, the interference fringes are imaged on a CMOS sensor and elaborated via a LabVIEW software. The system is also equipped with a four quadrant photodiode PD, which eventually can also be used. The description of the process of retrieving the phase of the interferometer from the image of the fringes will be presented in a dedicated paper.

All the optical components of the UINT interferometer are fixed on a circular plate of 210 mm diameter, placed in an aluminium vacuum temperature-controlled chamber C, where the standard pressure p is generated. The whole optical system and the chamber C are shown in Fig. 2.

The interferometer was designed to minimize mechanical deformations due to eventual temperature variations and gradients. In particular, the double mirror assembly and the circular plate on which this assembly is bonded, are made both of ZERODUR® glass ceramic, material characterized by extremely low-thermal-expansion, that is also homogenous throughout the entire bulk volume, making it suitable for high-demanding applications in terms of intrinsic thermo-mechanical
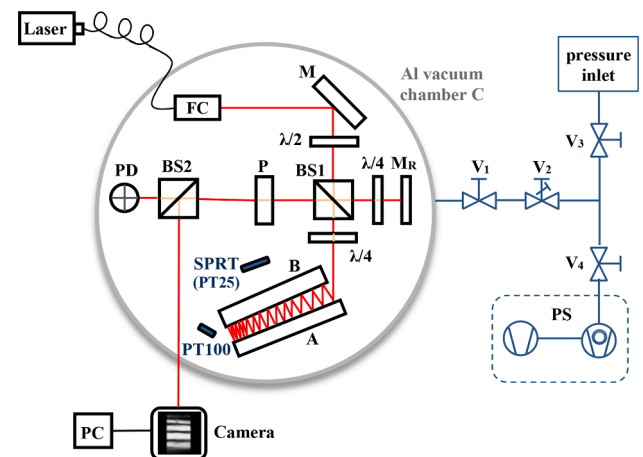

Fig. 1. Schematic of the UINT optical pressure standard with laser interferometer placed inside aluminium vacuum chamber C; V$_1$: vacuum chamber valve; V$_2$: variable leak valve; V$_3$: inlet system valve; V$_4$: pump valve; PS: pumping system.
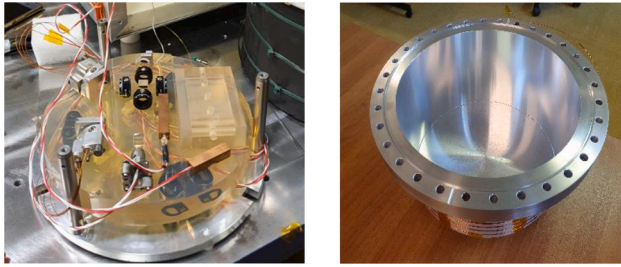
Fig. 2. Left: UINT optical pressure standard; right: aluminium vacuum chamber hosting interferometer.

stability: the nominal mean coefficient of thermal expansion (CTE) within the temperature range of 0 °C to 50 °C is equal to $0 \pm 0.050 \times 10^{-6}$/K.

In a previous preliminary realization [21,22] the two mirrors were made of Clearceram® directly bonded to a plate made of the same material, allowing a maximum unbalance of about 1.5 m. The UINT Zerodur® double mirror assembly was instead built following a different approach: it was designed and initially realized as a stand-alone device, bonding the two mirrors to a spacer (Fig. 3), in order to obtain a "multi-reflection cavity" that could eventually be used for different experiments. This cavity, of total dimension equal to $(90 \times 60 \times 27)$ mm and able to achieve an optical path of more than 6 m, was successively bonded to the 210 mm diameter circular plate; the latter was placed on suitable kinematic spherical supports to minimize mechanical stresses and vibrations during gas inlet or pumping process.

The mirrors were realized with protected silver coating, to allow an optimal compromise between highest reflectance in the visible spectrum and minimum effect in terms of penetration depth of the laser beam on the mirror surface and to obtain a device which was also suitable to be used at different wavelength, in particular at the green wavelength.

The purpose of the quasi-monolithic mirror assembly is to aim to the maximum mechanical stability, hence the maximum stability of the unbalance of the interferometer. It could be observed that the length of the optical path is not uniquely defined and can slightly change, e.g. by translating or rotating the entering beam. On the other hand, the alignment of the interferometer is quite critical and the boundary conditions to get the interference fringes are very strict. Furthermore, the stability of the entrance beam is guaranteed by the quality of the mounting of the optical components, from the fiber collimator, to the mirrors, to the retarder plates and the beam splitters. The repeatability of the experimental data supports this hypothesis.

The UINT realization benefits from a series of optical simulation studies conducted to optimize its design, in particular to achieve a predictive estimate of the nominal optical path in the measurement arm of the interferometer and to predict the value of misalignment between the entrance and the exit laser beam, i.e. to evaluate the distance between the laser spots correspondent to the entrance and the exit laser beam, as function of tilt angle along the x-axis, in which the multiple reflections on mirrors occur. The nominal optical path in the double mirror cavity was predicted through a ray-tracing study implemented in python™ ambient; the Gaussian beam study to estimate the misalignment between the entrance and the exit laser beam was implemented in Zemax OpticStudio®. The following parameters were adopted, according to the technical drawings of double mirror assembly: angle $\beta = 0.025°$ between the mirrors A and B in the plane xy, incident laser beam at angle $\alpha = 2°$ to the perpendicular to the xz plane, a nominal distance of $H = 40$ mm between the mirrors at the entrance of the beam inside the double mirror assembly and a beam size of 0.96 mm (Gaussian beam 1/e^2). The simulation was set to have the total number of reflections on the mirrors over a length of 60 mm along the x-axis, which is conservative, considering the useful length of 70 mm, correspondent to the size of rectangular slot of the spacer.

The predictive estimate L_{pred} of the unbalance, as function of incident angle of laser beam, is shown in Fig. 4, where, for each point of the figure, the value of optical path difference outside the double mirror assembly was added at each predicted value of the optical path inside the double mirror assembly determined by the simulation.

For the nominal values of relevant parameters β, α and H, the predicted value of the unbalance is $L_{pred} = (6478.65 \pm 0.02)$ mm, where the dominant source of uncertainty is due to the estimate of the optical path difference outside the double mirror assembly.

It should be noted that the aforementioned result was obtained using the nominal geometrical parameters, according to the technical drawings of the double mirror multiplication set-up, therefore the value L_{pred} has to be compared with the experimental result L, to estimate the real values of parameters β, α and H. The experimental value of unbalance, without taking into account the penetration depth, as discussed in Section 4.3, is $L = (6320.94 \pm 0.04)$ mm. For the nominal values of parameters β and H (Fig. 4, left) the value at angle $\alpha = 1.95°$ has a relative difference equal to $3.5 \cdot 10^{-4}$; adjusting the parameter H (Fig. 4, right) at the value 39.97 mm, the relative difference is only $3.2 \cdot 10^{-6}$.

Beside the predicted value L_{pred} of the unbalance, a Gaussian beam propagation study was carried out to predict the value of misalignment between the entrance and the exit laser beam. The Fig. 5 shows the systematic effect of eventual manufacturing defect of double mirror cavity, that is the misalignments between entrance and exit beam due to tilt angle θ along x-axis, to take into account the possible deviation from parallel condition of reflecting surfaces (plane xz) of the two mirrors. Due to small size of the laser beam entrance hole on mirror A (only 6 mm diameter), the results shown in Fig. 5 demonstrates that, conservatively, a maximum tilt angle of 0.0004° can be accepted: as consequence, to make negligible this systematic effect, a custom procedure was adopted by the manufacturer during the realization of the cavity.

After the design phase, the system was realized in accordance with the schematic shown in Fig. 2 and equipped with a custom software
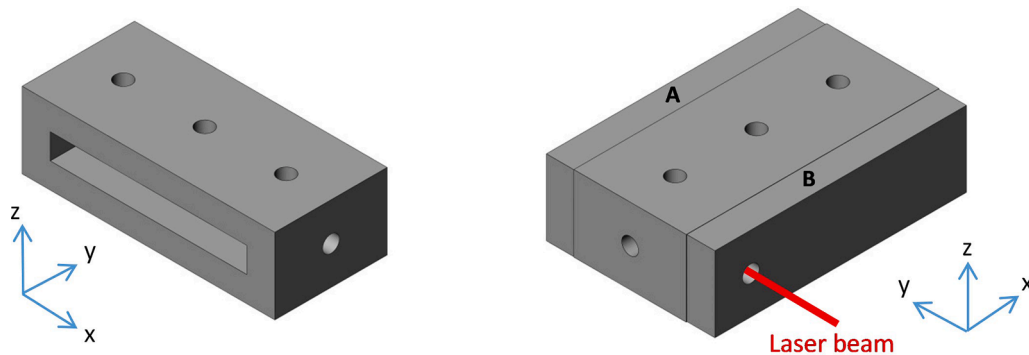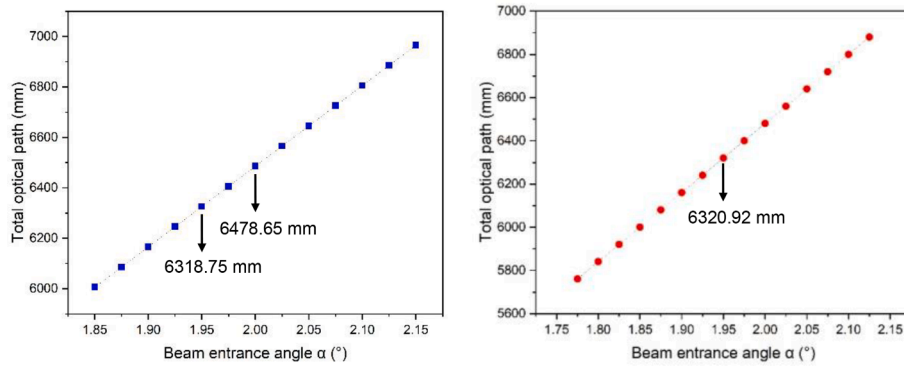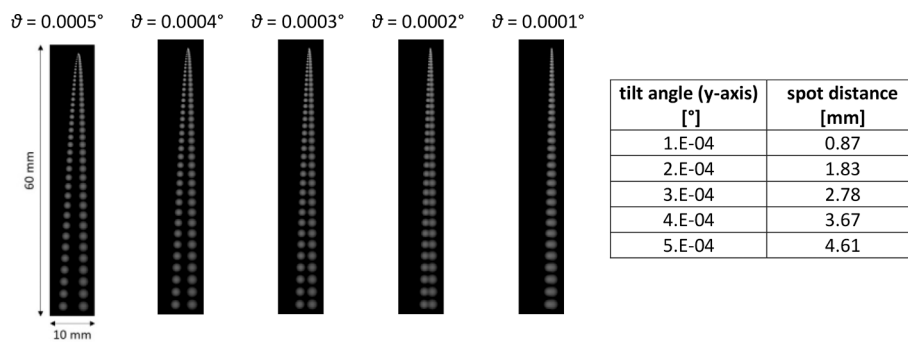

Fig. 3. Multi-reflection double mirror cavity. Left: Zerodur® spacer with rectangular slot and circular holes for gas inlet; right: Zerodur® double mirror assembly (spacer with quasi-parallel mirrors A and B).

Fig. 4. Ray-tracing study implemented in python™ ambient: predictive estimate of the unbalance L_{pred} as function of incident angle. Left: L_{pred} calculated at the nominal values of relevant parameters β, α and H. Right: L_{pred} calculated at the adjusted values of relevant parameters β, α and *H*, after the experimental measurement of unbalance L (Section 4.3).

tilt angle (y-axis) [°]	spot distance [mm]
1.E-04	0.87
2.E-04	1.83
3.E-04	2.78
4.E-04	3.67
5.E-04	4.61

Fig. 5. Zemax OpticStudio® simulation: misalignments between entrance and exit beam due to tilt angle along x-axis.

implemented in LabVIEW ambient, which manages the acquisition of data.

4. Results

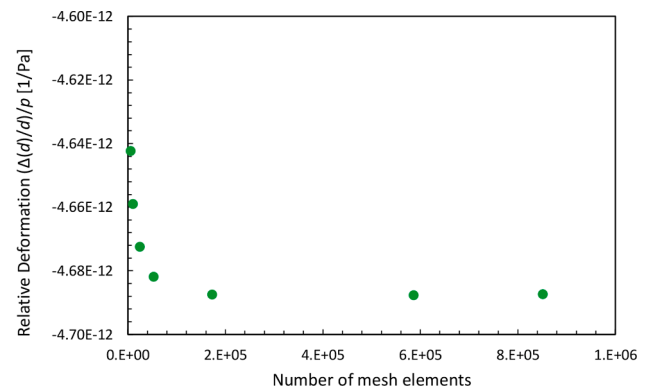### 4.1. The FEM analysis of the double mirror assembly

The realization of a photonic pressure standards based on the refractive index measurement depends on various factors affecting its accuracy, among which there is the systematic effect of gas pressure on the mechanical deformation of the optical cavities. Such effect is pressure-dependent and is strictly related to the specific adopted optical cavity, that is, in our case, the double mirror assembly previously described. The cavity deformation can be estimated by means of finite element method (FEM), as reported in [28].

Before implementing the FEM model of the double mirror assembly, a propaedeutic work has been performed in the framework of EMPIR project 18SIB04 "QuantumPascal" [29]: four partner of the project simulated the pressure-induced deformation of a given Fabry-Pérot cavity using their own independent methods with the aim of mutually validating these methods before undertaking the simulation of their own cavity. The results demonstrated a good agreement between the various partners with such small differences that methodological errors of the simulation procedure eventually contribute to a sub-ppm uncertainty in the assessments of refractivity.

Afterwards, the FEM analysis was implemented assuming an isotropic linear elastic model, applied to the double mirror assembly, using COMSOL Multiphysics® 5.5, a commercial software package for simulation of physics processes. The following parameters were introduced in the model for the relevant mechanical properties of Zerodur® material: density ρ = 2530 kg m^{-3}, Young's modulus E = 90.3 GPa, Poisson's ratio ν = 0.24. The boundary conditions were implemented in

accordance with the real physical conditions of the device, i.e. the constraint has been applied on the basis of the spacer. The gas pressure was introduced in the model using the "boundary load" tool of COMSOL structural mechanics module, choosing the correspondent load type "pressure".

During the preliminary activity described in [29] it was found that there is an evident dependence of the pressure-induced deformation on the number of mesh elements. Therefore, the study was carried out using different mesh sizes in order to evaluate the eventual influence of this parameter on the accuracy and convergence of the solution; different simulations were performed adopting $5.6 \cdot 10^3$ to $8.5 \cdot 10^5$ tetrahedral mesh elements: the Fig. 6 shows the results in term of pressure-normalized relative deformation $(\Delta d/d)/p$ of the double mirror cavity, where Δd is the mean value of change in distance between the two reflecting surfaces of mirrors A and B induced by the presence of gas and

Fig. 6. Pressure-normalized relative deformation $(\Delta d/d)/p$ of double mirror assembly at z = 0 for different size of mesh elements.

d is the distance between the mirrors at pressure *p* = 0.

The figure clearly evidence that the results of the FEM analysis converge for a number of mesh elements greater than $1.7 \cdot 10^5$, hence the deformation was estimated as average of the last three values occurred at higher number of mesh elements. The values reported in the Fig. 6 were obtained using a tool of COMSOL Multiphysics® 5.5, to calculate the average distance between two segments, i.e. the two segments, each of which is the locus of the points where the laser is reflected by each mirror forming the double-mirror cavity.

The uncertainty of the pressure-induced deformation was evaluated taking into account the relevant contributions due to the repeatability, the implemented model and the material.

The contribution due to repeatability, equal to $2.7 \cdot 10^{-16}$ Pa^{-1}, was calculated according to [30], to properly take into account the small amount of used data (N = 3). It has to be noted that with the hypothesis of uniform distribution of data, the repeatability would have been equal to $1.2 \cdot 10^{-16}$ Pa^{-1}: to be conservative, we decided to use the approach reported in [30], obtaining a "more prudent" higher uncertainty value.

A contribution of uncertainty due to the implemented model was considered: it was deduced from ref. [29] and equal to $1.5 \cdot 10^{-16}$ Pa^{-1}.

To take into account the uncertainty arising from a "not perfect" knowledge of the material used to realize the multi-reflection cavity, we implemented further FEM simulations in COMSOL, to evaluate the effect due to an eventual error of 1 % in the values of relevant parameters influencing the simulation (Young's modulus, Poisson's ratio and density): the correspondent error in the determination of the pressure-induced deformation was fully considered as uncertainty contribution, resulted equal to $8.3 \cdot 10^{-14}$ Pa^{-1}, and conservatively approximated to $1 \cdot 10^{-13}$ Pa^{-1}.

It should be noted that such uncertainty value corresponds to a relative change in the unbalance value *L,* at 100 kPa, equal to $1 \cdot 10^{-8}$, which can be considered negligible and was not cited in the Table 1, where only the relevant sources of uncertainty are mentioned.

The pressure-induced deformation resulted equal to (-4.7 $\cdot 10^{-12}$ ± $1 \cdot 10^{-13}$) Pa^{-1}.

4.2. The temperature control and measurement

The realization of an accurate optical-based pressure standard with a target relative uncertainty of 10 ppm at 100 kPa requires an assessment of temperature with an uncertainty not exceeding the value of 3 mK: to fulfil this requirement, a temperature control unit for UINT system was designed and realized.

The UINT system was placed inside a custom aluminum UHV vacuum chamber, that, compared to traditional stainless steel chamber, has the advantage of a greater thermal conductivity, enabling the realization of a higher performance thermal control. The aluminum technology also ensures optimal vacuum and thermal properties at reasonable costs compared to the eventual use of Oxygen-free high thermal conductivity (OFHC) copper. The chamber has internal diameter equal to 240 mm and height of 145 mm; the vacuum ports are all positioned in the closing flange (DN250 CF).

The system for thermal control was designed to have a double stage temperature stabilization.

To implement the first stage of control, the vacuum chamber containing the UINT system was placed in an aluminum box of dimensions equal to (38 × 38 × 34) cm, as showed in Fig. 7. Each face of the box was covered with an enameled manganin heater wire with nominal diameter of 0.6 mm and electrically insulated by adhesive Kapton tape. The wire was distributed over the surface in order to cover it uniformly, obtaining a total resistance equal to 68.1 Ω.

The aluminum box was internally covered with insulating material (extruded polystyrene with a thickness of 20 mm), which acts as thermal insulation between the external box and the vacuum chamber. A PT100 platinum resistance thermometer (PID_ext) was positioned in contact with an internal aluminum face of the box to measure and control the
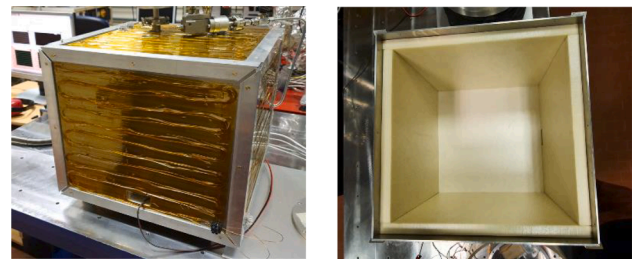

Fig. 7. Aluminum box for implementation of first stage of thermal control.

temperature of the box; the temperature of the box is regulated through a digital PID (Proportional Integral Derivative) control, using feedback from the PT100 sensor to calculate and adjust the power sent to the distributed resistance acting as actuator.

A second stage of control was implemented to manage the fine regulation of temperature by the same approach used for the first step of control: the external surface (lateral surface and base) of aluminum cylindrical vacuum chamber was also equipped with the enameled manganin heater electrically insulated by adhesive Kapton tape, reaching a total resistance of 33.2 Ω (Fig. 8). The PT100 platinum resistance thermometer (PID_int) to be used for second step of thermal control was placed along the lateral surface of the vacuum chamber at half height. The lateral surface and the base of the chamber were covered by armaflex insulating material.

The digital two PID controls are implemented in a LabVIEW program where the two temperatures are read with a GPIB protocol from two Keithley 2700 multimeters in a 4-wire configuration with a 1-second time interval. The correction signal is generated with the two analog outputs of a board NI PCI-6251 connected to a buffer circuit using a Darlington BDX53B connected to a 30 V voltage supply.

The UINT system was equipped with two different calibrated temperature sensors: a custom made PT100 sensor (single wire wound, with ceramic capsule) and a glass capsule SPRT PT25 Fluke 5686-B, both ITS90 compliant. Each temperature sensor of UINT system is connected to a dedicated digital 8.5 digit multimeter (HP 3458A). A LabVIEW software acquires the temperature of the PT100 and the PT25.

The vacuum chamber is also connected to two capacitance diaphragm gauges (respectively 10 Torr and 1000 Torr Full scale), a vacuum gauge for the measurement of residual pressure and a barometer.

The initial phase of measurement operations is the evacuation of the vacuum chamber to reach at least a residual pressure in the 10^{-2} Pa range. Subsequently the two steps of thermal control are switched on: the set points of temperature of the internal stage (aluminum vacuum chamber) and the external stage (aluminum box) are generally regulated to have a temperature difference of at least 1 °C. The double-stage thermal control is currently able to operate at a nominal final temperature set-point (internal stage) between 20 °C and 30 °C.

When the system has reached the optimal thermal stability in vacuum, the gas is entered in the chamber until the desired target pressure is reached.

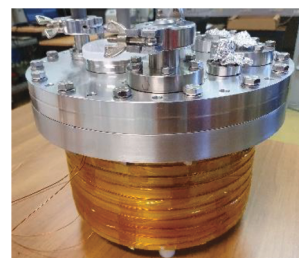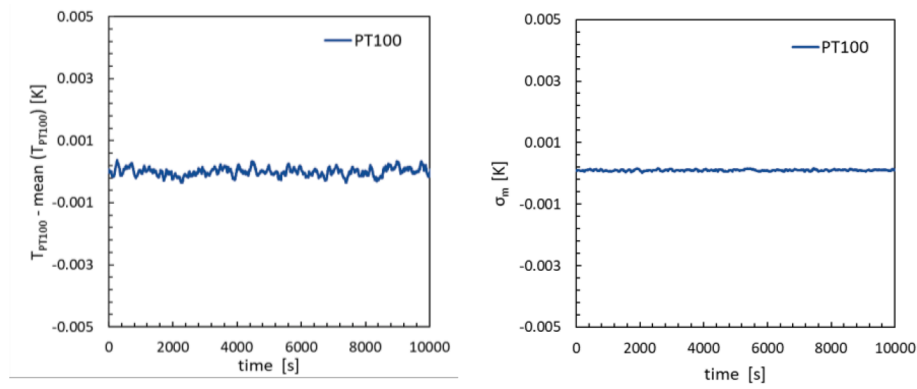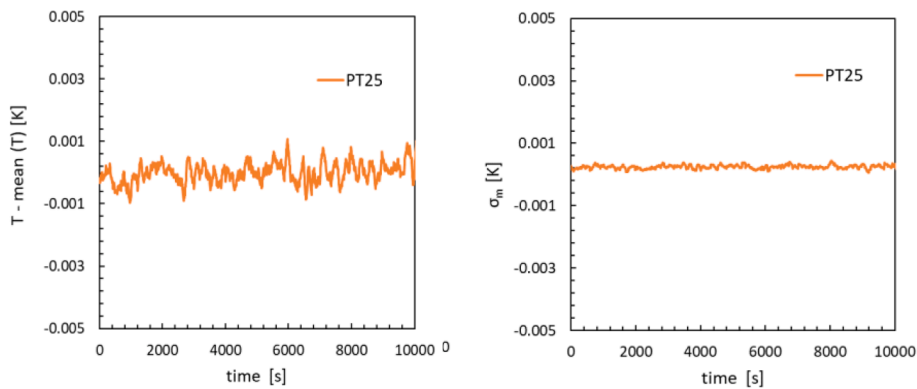The following Figs. 9 and 10 show the results of temperature stability

Fig. 8. UHV aluminum vacuum chamber with second stage of thermal control.

Fig. 9. PT100 sensor (double step thermal control, 100 kPa). Left: difference between temperature (mean value, 100 s) and its mean value over $1 \cdot 10^4$ s; right: standard deviation of the mean σ_m.

Fig. 10. PT25 sensor (double step thermal control, 100 kPa). Left: difference between temperature (mean value, 100 s) and its mean value over $1 \cdot 10^4$ s; right: standard deviation of the mean σ_m.

over a time of $1 \cdot 10^4$ s respectively for the PT100 and the PT25: the reported temperatures are calculated as a mean over 100 s, as well as the standard deviations of the mean.

To evaluate the repeatability of the temperature measurement, a mean value of 100 s has been considered as a typical duration of each measurement of UINT system at the reached target pressure point (100 kPa).

The obtained results show that the implemented thermal control is able to maintain the temperature stability within ± 1 mK for both the PT100 and PT25 sensors with standard deviations in the sub-millikelvin range. In particular, the measurements carried out with PT100 sensor exhibit a stability within ± 0.5 mK with a standard deviation of the mean not exceeding 0.2 mK.

The Fig. 11 evidences the temperature differences measured by PT100 sensor and SPRT PT25 with double step thermal control fully operational at 100 kPa.

It should be noted that the SPRT PT25 was placed approximately at the centre of the UINT system, practically at a distance of about 100 mm from the heated lateral surfaces of the cylindrical vacuum chamber; the PT100 sensor was positioned close to the double mirror assembly at about 20 mm from the aforementioned heated surfaces of the chamber. Thereby, the difference of temperature measured by the two thermometer provides a first estimate of both the intrinsic different readings (for example due to calibration) and the thermal gradients of the chamber at the height in which the optical and optomechanical components of UINT have been positioned.
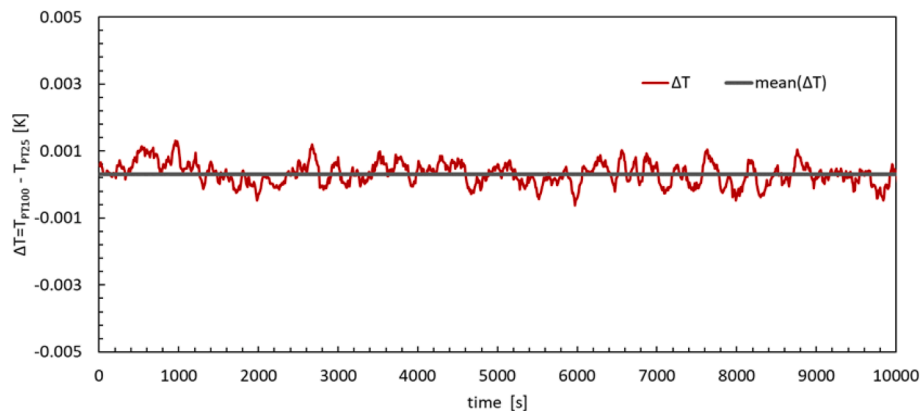
Fig. 11. Temperature difference ΔT measured by PT100 sensor and SPRT PT25 with double step thermal control at 100 kPa.

Beside the temperature control described above, to further check the thermo-dynamics conditions of the system, the pressure stability can be also estimated before the acquisition of the interferometric fringes and the temperature, typically by means of the barometer connected to UINT system for a time up to 240 s (60 s are generally enough). The Fig. 12 shows of an example of a measurement at nominal pressure 90 kPa, for a time of 60 s (sampling interval 0.25 s) by means of the barometer:

In addition, beside the determination of the unbalance of the interferometer, a preliminary study was carried out to test the performance of the UINT system, when used as a pressure sensor, evaluating its response in terms of sensitivity S, i.e. the ratio $\Delta p/\varphi$, where Δp is the difference between the pressure measured by a barometer (uncertainty equal to 2.8 Pa) corrected for the residual pressure and φ is the total number of fringes detected during the pressure variation Δp.

The Fig. 13 shows the results of the relative variations of the ratio $\Delta p/\varphi$ in the pressure range between 70 kPa and 100 kPa for nitrogen and helium: the results are within $\pm$ 20 ppm for nitrogen and to a large extent within $\pm$ 30 ppm for helium.

4.3. The unbalance of the interferometer

The essential precondition to put into operation the UINT system as primary optical pressure standard is the determination of the unbalance L of the interferometer under vacuum, i.e. the optical path difference between reference and measurement arm of the interferometer, which requires a dedicated experimental set up.

The unbalance of the UINT system was determined by means of a technique based on the frequency scanning interferometry (FSI) [31,32], where the accumulated phase difference is measured while the frequency ν of the laser is scanned, resulting in an induced Φ proportional to the unbalance L through the formula:

$$\Delta\Phi = \frac{n\Delta\nu L}{c} \tag{7}$$

where L is the unbalance of the interferometer, $\Delta\Phi$ is the accumulated phase expressed in cycles, $\Delta\nu$ is the total frequency scan interval and n is the refractive index. As consequence, the determination of the unbalance L through the equation (7) substantially depends only by the total frequency interval and the accumulated phase shift, assuming that the refractive index n can be approximated to 1, as the measurement of the unbalance is carried out in vacuum.

The technique was implemented according to the scheme reported in Fig. 14.

The laser source, a tunable diode laser (New Focus Vortex 6000), is scanned in frequency by about 45 GHz by sending a voltage ramp to its PZT input by means of an external function generator. After passing
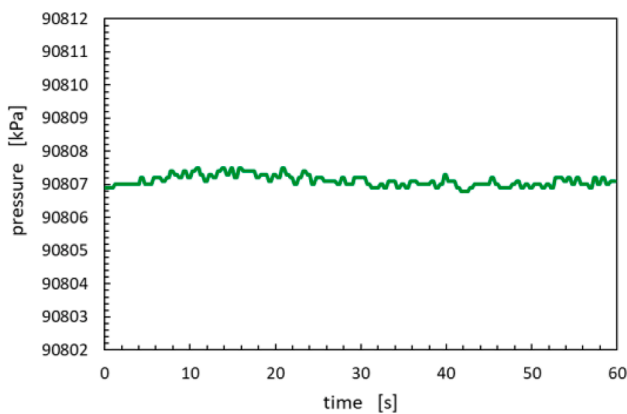

Fig. 12. Pressure measured by a barometer to check the pressure stability before the interferometric fringes acquisition (standard deviation of the mean $u_A = 0.011$ Pa).

through a Faraday optical isolator, the laser beam is launched in one of the inputs of a fiber splitter: one of the outputs is sent to the UINT system, where the accumulated phase is measured; the second output is sent to a calibrated wave meter, which is used for the determination of the frequency scan amplitude $\Delta\nu$. The wavemeter is a modified LM-10 lambdameter, originally developed by NIST, where the absolute frequency measurement may be performed with time interval from 1 s to 10 s, depending on the requested resolution. Since the wavelength of the scanning Vortex laser is close to the wavelength of the reference laser (the difference is about 0.1 nm), there is no need to correct for the index of refraction of air. Moreover, since in equation (7) only the scan amplitude $\Delta\nu$ is considered, the possible systematic effects are largely cancelled out in the difference calculation, but in order to be conservative, we still evaluated an associated uncertainty of 250 kHz. We performed six independent measurements of the unbalance of the UINT system, obtaining a mean value equal to L = 6320.94 mm, which is the value to be compared with the predictive estimate reported in Section 3.

In addition, the effect of penetration depth on the mirrors was considered, assuming a penetration depth of 50 nm: for a typical number of reflections equal to 156 (forward and backward optical path), the corrected value of the unbalance L resulted equal to (6320.93 $\pm$ 0.04) mm, where the relevant contributions to the uncertainty are basically due to frequency scan and accumulated phase measurements, the repeatability and, to a lesser extent, to the penetration depth effect.

The repeatability resulted equal to 0.016 mm: it has been evaluated by the standard deviation of the mean of the six independent measurements of the unbalance and conservatively corrected to take into account the limited number of measurement, as reported in [33].

The contributions due to frequency scan and accumulated phase measurements are respectively 0.035 mm and 0.015 mm.

The uncertainty due to the penetration depth correction is equal to 0.004 mm: we assumed a uniform distribution with (a+ − a−) = 80 nm where a+ = +40 nm and a− = −40 nm are respectively the upper and lower limit of the distribution.

As discussed in Section 3, the result of L is in agreement with the predicted value of the unbalance L_{pred}, setting the parameter H, i.e. the thickness of the spacer, at the value 39.97 mm.

5. The uncertainty budget

The model equation for the uncertainty evaluation is represented by equation (5), where the refractive index n and its uncertainty are determined according to equation (4).

The quantities involved in the calculation of the refractive index are the number of interference fringes φ occurred between the initial residual pressure p_{res} and p, the laser wavelength λ and the unbalance L under vacuum.

The number φ is determined on the basis of what has been reported in [21]. The description of the process of retrieving the phase of the interferometer from the acquired image of the fringes will be presented in a dedicated paper. The current standard uncertainty is $1.4 \cdot 10^{-3}$ fringes.

The laser source is a SIOS SL-03 He-Ne laser calibrated at INRIM against the national reference standard; the uncertainty (k = 1) of its wavelength is equal to $2 \cdot 10^{-13}$ m.

The method for the measurement of the unbalance L is described in the Section 4.3: the obtained standard uncertainty is 0.04 mm.

After the determination of the refractive index and its uncertainty, the equation (5) can be applied for the calculation of the standard pressure, as well as its uncertainty.

The temperature control and measurement are described in Section 4.2. The standard uncertainty is 1.4 mK, taking into account calibration, repeatability and temperature gradients inside the vacuum chamber in which the UINT system is placed.

The molar refractivity A_R for nitrogen adopted in the present work is derived from [34]: its standard uncertainty is equal to $2 \cdot 10^{-11}$ m^3/mol.
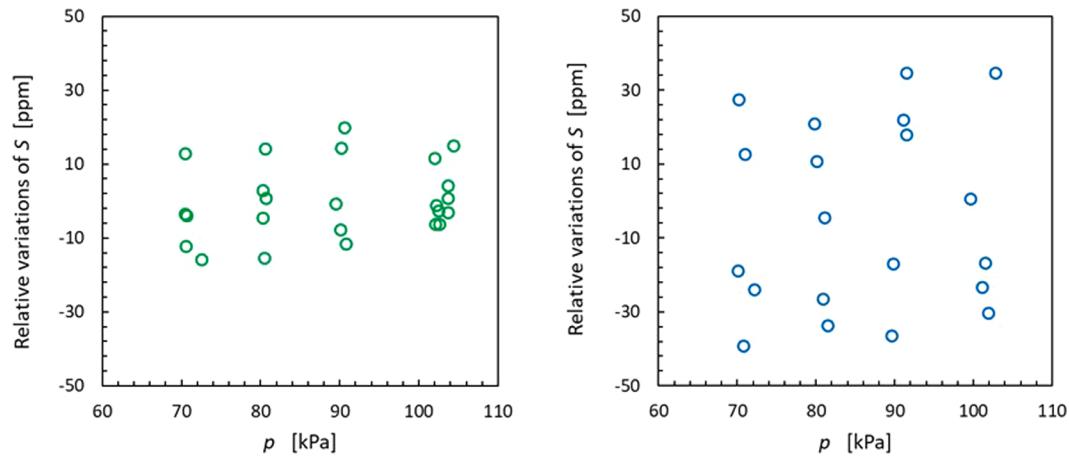
Fig. 13. Relative variation of ratio between pressure over the number of fringes in the range 70 kPa to 100 kPa. Left: results for nitrogen; right: results for helium.
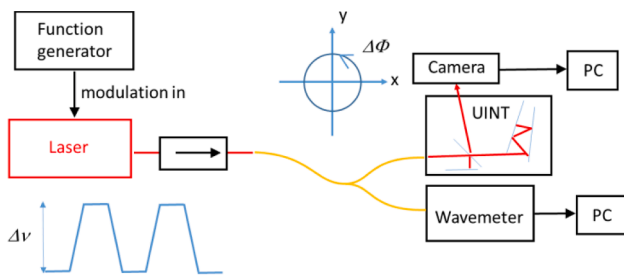

Fig. 14. Schematic of the frequency scanning interferometry-based technique for the determination of the unbalance L of the interferometer (UINT) under vacuum conditions.

The second and third order density virial coefficients B and C and their uncertainties are determined according to [34,35]; the standard uncertainties are respectively $u(B) = 1 \cdot 10^{-7}$ m^3/mol and $u(C) = 1 \cdot 10^{-10}$ m^6/mol^2.

The second and third order refractivity virial coefficients B_R and C_R and their uncertainties are obtained according to [34,36]; the standard uncertainties are respectively $u(B_R) = 1 \cdot 10^{-13}$ m^6/mol^2 and $u(C_R) = 5 \cdot 10^{-18}$ m^9/mol^3.

As example, the uncertainty budget at standard pressure $p = 101466.4$ Pa is summarized in the Table 1, where the main sources of uncertainty are shown.

Table 1
Example of uncertainty budget at $p = 101466.4$ Pa, nitrogen. The percentage in the last column is the relative contribution of each variance to the total variance.

Input x_i	Source of uncertainty	$|c_i\, u(x_i)/p_i|$	% Variance
n	Interference fringes φ, laser wavelength λ, unbalance L; eq. (4)	$6.36 \cdot 10^{-6}$	40.8 %
T	Calibration uncertainty, repeatability, temperature gradients	$4.62 \cdot 10^{-6}$	21.6 %
A_R	Molar polarizability [34]	4.50×10^{-6}	20.4 %
B	Second order density virial coefficient [34,35]	4.03×10^{-6}	16.4 %
B_R	Second order refractivity virial coefficient [34,36]	9.06×10^{-7}	0.8 %
C	Third order density virial coefficient [34,35]	1.62×10^{-7}	0.0 %
C_R	Third order refractivity virial coefficient [34,36]	1.83×10^{-9}	0.0 %
$(u_c(p)/p)$ $\cdot 10^6$		(combined relative standard uncertainty)	10 ppm

The UINT pressure standard has a relative standard uncertainty of 10 ppm at 100 kPa: compared to the previous realization [21,22] which uncertainty was at 100 ppm level, this result represents a substantial step forward towards an optical realization of the pascal through multi-reflection interferometry technique.

The relative standard uncertainty in the current operational range of the UINT system has been evaluated as reported in the following table:

The results in Table 2 show that the optimal working range of the UINT optical pressure standard is above 10 kPa where the relative uncertainty is 10 ppm; for pressure below 1 kPa the system appears to be less performing and its relative uncertainty is higher than 50 ppm.

The next upcoming important step will be to further check the performance of the UINT system by comparing it with traditional pressure standards available at INRIM, namely FPG (Force Balanced Piston Gauge and a pressure balance and evaluate the feasibility of extending the higher pressure operational limit to 200 kPa.

6. Conclusions

The paper presents the recent progress on the realization of an optical pressure standard operating up to 120 kPa, based on an unbalanced homodyne interferometer (UINT). A novel system has been designed and realized, including a new optical layout, to have one of the two arms of the UINT interferometer formed by a multi reflection double mirror assembly to establish an unbalance length L between the two arms larger than 6 m in a compact set-up.

The most important factors which could influence the performance of UINT have been studied, including the control of the temperature at millikelvin level and the measurement in vacuum of the unbalance of the interferometer, performed by an independent technique, allowing to use the system as absolute refractometer to realize an optical pressure standard, alternative to Fabry-Pérot cavities-based standards.

The uncertainty budget evidenced that the UINT pressure standard has currently a relative standard uncertainty of 10 ppm at 100 kPa, representing a considerable improvement, compared to the previous

Table 2
Relative standard uncertainties of UINT optical pressure standard.

p_{nom}	$u(p_{UINT})/p_{UINT}$
Pa	
100	5.2E−04
400	1.3E−04
1000	5.3E−05
3000	2.0E−05
10000	1.0E−05
$p > 10000$	1.0E−05

realization, which uncertainty was at 100 ppm level.

Further studies will be performed to test the performance of the UINT system by comparing it with traditional pressure standards available at INRIM and to evaluate its long term stability.

CRediT authorship contribution statement

D. Mari: Conceptualization, Methodology, Investigation, Validation, Formal analysis, Writing – original draft, Writing – review & editing, Visualization, Funding acquisition, Supervision. **M. Pisani:** Conceptualization, Methodology, Investigation, Validation, Formal analysis, Writing – review & editing. **M. Astrua:** Software, Investigation, Formal analysis, Writing – review & editing. **M. Zucco:** Software, Methodology, Investigation, Formal analysis, Writing – review & editing. **S. Pasqualin:** Resources, Writing – review & editing. **A. Egidi:** Software, Writing – review & editing. **M. Bertinetti:** Resources, Writing – review & editing. **A. Barbone:** Resources, Writing – review & editing.

Declaration of Competing Interest

The authors declare that they have no known competing financial interests or personal relationships that could have appeared to influence the work reported in this paper.

Data availability

The data are available at Zenodo Repository.

Acknowledgements

References

[1] C.G. Rendle, H. Rosenberg, Metrologia 36 (1999) 613–666.
[2] A. Ooiwa, Metrologia 30 (1994) 607–610.
[3] C.M. Sutton, M.P. Fitzgerald, Metrologia 46 (2009) 655–660.
[4] F. Alasia, G. Birello, A. Capelli, G. Cignolo, M. Sardi, Metrologia 36 (1999) 499–503.
[5] J. Könemann, S. Ehlers, M. Jescheck, W. Sabuga W, in: Proc. of 5th CCM Pressure Metrology & 4th IMEKO TC16 Int. Conf., Berlin, May 2–5, PTB-Mitteilungen 121: S (2011) 303–306.
[6] W. Jitschin, Metrologia 39 (2002) 249–261.
[7] M. Bergoglio, A. Calcatelli, Metrologia 41 (2004) 278–284.
[8] K. Jousten, H. Menzer, D. Wandrey, R. Niepraschk, Metrologia 36 (1999) 493–497.
[9] M. Bergoglio, D. Mari, Vacuum 84 (2009) 270–273.
[10] Word Health Organization Resolution WHA67.11. https://www.who.int/publications.
[11] P.F. Egan, J.A. Stone, J.K. Scherschligt, A.H. Harvey, J. Vac. Sci. Technol. A 37 (2019) 3.
[12] P.F. Egan, J.A. Stone, J.H. Hendricks, J.E. Ricker, G.E. Scace, G.F. Strouse, Opt. Lett. 40 (2015) 3945.
[13] P. Egan, J.A. Stone, Appl. Opt. 50 (2011) 3076.
[14] I. Silander, C. Forssén, J. Zakrisson, M. Zelan, O. Axner, J. Vac. Sci. Technol. B 39 (2021) 044201.
[15] J. Zakrisson, I. Silander, C. Forssén, M. Zelan, O. Axner, J. Vac. Sci. Technol. B 38 (2020), 054202.
[16] I. Silander, C. Forssén, J. Zakrisson, M. Zelan, O. Axner, Opt. Lett. 45 (2020) 2652.
[17] K. Jousten, et al., Metrologia 54 (2017) S146.
[18] Y. Yang, T. Rubin, J. Phys. Conf. Ser. 1065 (2018), 162003.
[19] D. Mari, M. Bergoglio, M. Pisani, M. Zucco, Meas. Sci. Technol. 25 (2014), 125303.
[20] M. Domenico, P. Marco, F. Claudio, Measurement: Sensors 18 (2021) 100253, doi: 10.1016/j.measen.2021.100253.
[21] D. Mari, M. Pisani, M. Zucco, Measurement 132 (2019) 402.
[22] D. Mari, M. Pisani, M. Zucco, J. Phys.: Conf. Ser. 1065 (2018), https://doi.org/10.1088/1742-6596/1065/16/162007.
[23] Z. Silvestri, D. Bentouati, P. Otal, J.-P. Wallerand, Acta IMEKO 9 (2020) 305.
[24] Y. Takei, K. Arai, H. Yoshida, Y. Bitou, S. Telada, T. Kobata, Measurement 151 (2020), 107090.
[25] P.M.C. Rourke, et al., Metrologia 56 (2019), 032001.
[26] P.M.C. Rourke, J. Phys. Chem. Ref. Data 50 (2021), 033104.
[27] M. Pisani, Meas. Sci. Technol. 20 (2009), 084008.
[28] T. Rubin, Y. Yang, J. Phys.: Conf. Ser. 1065 (2018), 162003.
[29] J. Zakrisson, I. Silander, C. Forssén, Z. Silvestri, D. Mari, S. Pasqualin, A. Kussicke, P. Asbahr, T. Rubin, O. Axner, Acta IMEKO 9(5) (2020) 281, ISSN 2221-870X.
[30] K. Jousten, et al., Metrologia 57 (2020) 07031, https://doi.org/10.1088/0026-1394/57/1A/07031.
[31] A. Cabral, J. Rebordao, Opt. Eng. 46 (7) (2007) 73602.
[32] P.A. Coe, D.F. Howell, R.B. Nickerson, Measur. Sci. Technol. 15 (11) (2004) 2175–2187.
[33] R. Kacker, A. Jones, Metrologia 40 (2003) 235.
[34] P.F. Egan, J.A. Stone, J.E. Ricker, J.H. Hendricks, Rev. Sci. Instrum. 87 (2016), 053113, https://doi.org/10.1063/1.4949504.
[35] J.D. Dymond, K.N. Marsh, R.C. Wilhoit, K.C. Wong, Virial Coefficients of Pure Gases and Mixtures, Springer-Verlag, Berlin, 2002.
[36] H.J. Achtermann, G. Magnus, T.K. Bose, J. Chem. Phys. 94 (8) (1991) 5669–5684.